



The Oeschinensee rock avalanche, Bernese Alps, Switzerland: a co-seismic failure 2300 years ago?

Patrizia Köpfli¹ · Lorenz M. Grämiger¹ · Jeffrey R. Moore^{1,3} · Christof Vockenhuber² · Susan Ivy-Ochs²

Received: 8 June 2017 / Accepted: 15 December 2017 / Published online: 16 January 2018
© Swiss Geological Society 2017

Abstract

Landslide deposits dam Lake Oeschinen (Oeschinensee), located above Kandersteg, Switzerland. However, past confusion differentiating deposits of multiple landslide events has confounded efforts to quantify the volume, age, and failure dynamics of the Oeschinensee rock avalanche. Here we combine field and remote mapping, topographic reconstruction, cosmogenic surface exposure dating, and numerical runout modeling to quantify salient parameters of the event. Differences in boulder lithology and deposit morphology reveal that the landslide body damming Oeschinensee consists of debris from both an older rock avalanche, possibly Kandertal, as well as the Oeschinensee rock avalanche. We distinguish a source volume for the Oeschinensee event of 37 Mm³, resulting in an estimated deposit volume of 46 Mm³, smaller than previous estimates that included portions of the Kandertal mass. Runout modeling revealed peak and average rock avalanche velocities of 65 and 45 m/s, respectively, and support a single-event failure scenario. ³⁶Cl surface exposure dating of deposited boulders indicates a mean age for the rock avalanche of 2.3 ± 0.2 kyr. This age coincides with the timing of a paleo-seismic event identified from lacustrine sediments in Swiss lakes, suggesting an earthquake trigger. Our results help clarify the hazard and geomorphic effects of rare, large rock avalanches in alpine settings.

Keywords Rock avalanche · Landslide-dammed Lake · Cosmogenic ³⁶Cl dating · Runout modeling · Seismic triggering · Swiss Alps

1 Introduction

Large valley-blocking landslides represent a considerable hazard to mountain communities through the combined effects of rapid release and runout of slide debris, as well as lake formation, inundation, and potential for catastrophic outburst flooding (Heim 1932; Evans et al. 2011). Defined by the sudden release of large intact-rock volumes, rock avalanches (*sensu* Hungr et al. 2001) can achieve runout velocities in excess of 90 m/s with flow-like movement and

immensely destructive power (Crosta et al. 2004; Pankow et al. 2014). Such events, while rare, have been responsible for large losses of life in the past, and many are associated with strong ground shaking accompanying large earthquakes (Dunning et al. 2007; Kuo et al. 2011; Wolter et al. 2016). Meanwhile, river-blocking landslide barriers are poorly suited for long-term stability and frequently breach shortly after their formation; only ~ 15% last longer than a year (Costa and Schuster 1988; Suter 2004). One of the greatest landslide disasters in history resulted from breach of a landslide dam: in 1786 an earthquake-triggered rock-slide blocked the Dadu River in China, creating a dam which failed 10 days later and released a flood that killed an estimated 100,000 people (Dai et al. 2005).

In contrast to their hazard, valley-blocking landslides are also responsible for creating some of the world's most striking landscapes, forming lakes, meadows and gentle parcels of land amidst high-relief terrain (Hewitt et al. 2011; Castleton et al. 2016). Oeschinensee in the Bernese Alps of Switzerland is a stunning, classical example of a landslide-dammed lake (Heim 1932; Abele 1974; Bonnard

Handling Editor: W. Winkler

✉ Jeffrey R. Moore
jeff.moore@utah.edu

¹ Department of Earth Sciences, ETH Zurich, Sonneggstrasse 5, 8092 Zurich, Switzerland

² Ion Beam Physics, ETH Zurich, Otto-Stern-Weg 5, 8093 Zurich, Switzerland

³ Department of Geology and Geophysics, University of Utah, 115 S 1460 E, Salt Lake City, UT 84112, USA

2011). Located high in a glaciated catchment above the Village of Kandersteg (Fig. 1), the striking scenery of milky blue water surrounded by cascading glaciers and serrated peaks has attracted tourists and scientists alike for nearly 150 years (Murphy 1874; Taylor 1893). Today the Oeschinensee is part of the Swiss Alps Jungfrau-Aletsch UNESCO World Heritage site.

Quaternary geology in this region is dominated by the Kandertal rock avalanche, a 12 km long deposit of crushed rock left from one of the largest known Alpine rock slope failures (Heim 1932). First interpreted as glacial deposits, Penck and Brückner (1909) recognized the landslide character of the Kandertal deposits in light of fresh outcrops from the construction of railroad lines. Prevailing theories at that time placed the Kandertal rock avalanche as syn-glacial (i.e. occurring in the presence of a glacier) and therefore occurring during the Alpine Lateglacial period (c. 19–11.7 ka; Reitner et al. 2016), while the neighboring younger Oeschinensee rock avalanche and lake were described only as post-glacial (Turnau, 1906). Today, we know the Kandertal rock avalanche (also known as the Fisistock event) dates to ~ 9500 cal year BP and had a volume of about 800 million m^3 (Tinner et al. 2005). The Kandertal event is, in fact, thought to have consisted of two phases: (1) a rock avalanche which blocked water flowing through the Kandertal and formed a temporary lake, and (2) a lake outburst flood with subsequent debris flow running out a maximum distance of 15 km some 200–500 years later (Tinner et al., 2005).

Landslide debris damming Oeschinensee (Fig. 1) has traditionally been mapped as a single deposit (e.g. Furrer et al. 1993). Niklaus (1967) determined the volume of the landslide deposit to be 110 million m^3 , with a runout distance of 1 km, and estimated the age of lake formation as ~ 8000 yrs BC (Niklaus 1967). In contrast, Turnau (1906) estimated the landslide had a volume of only $\sim 50,000$ m^3 with a runout distance of 500 m. The large difference in these volumes relates to the assumed extent of the Oeschinensee rock avalanche deposit and whether this encompasses the complete mass of debris that blocks the lake or just the eastern portion (described in further detail below). Therefore, the question of the definition of the Oeschinensee landslide deposits has existed since the beginning of geological research in this area.

Despite the prominence of Oeschinensee as an archetype of landslide-dammed Alpine lakes, past studies have not been able to conclusively identify the extent, volume, age, and dynamics of the valley-blocking Oeschinensee rock avalanche. Several key questions remain, such as when did the Oeschinensee rock avalanche occur, did it have an attributable trigger, what was the volume and extent of the source and deposit, and how are these deposits stratigraphically related to the neighboring Kandertal event?

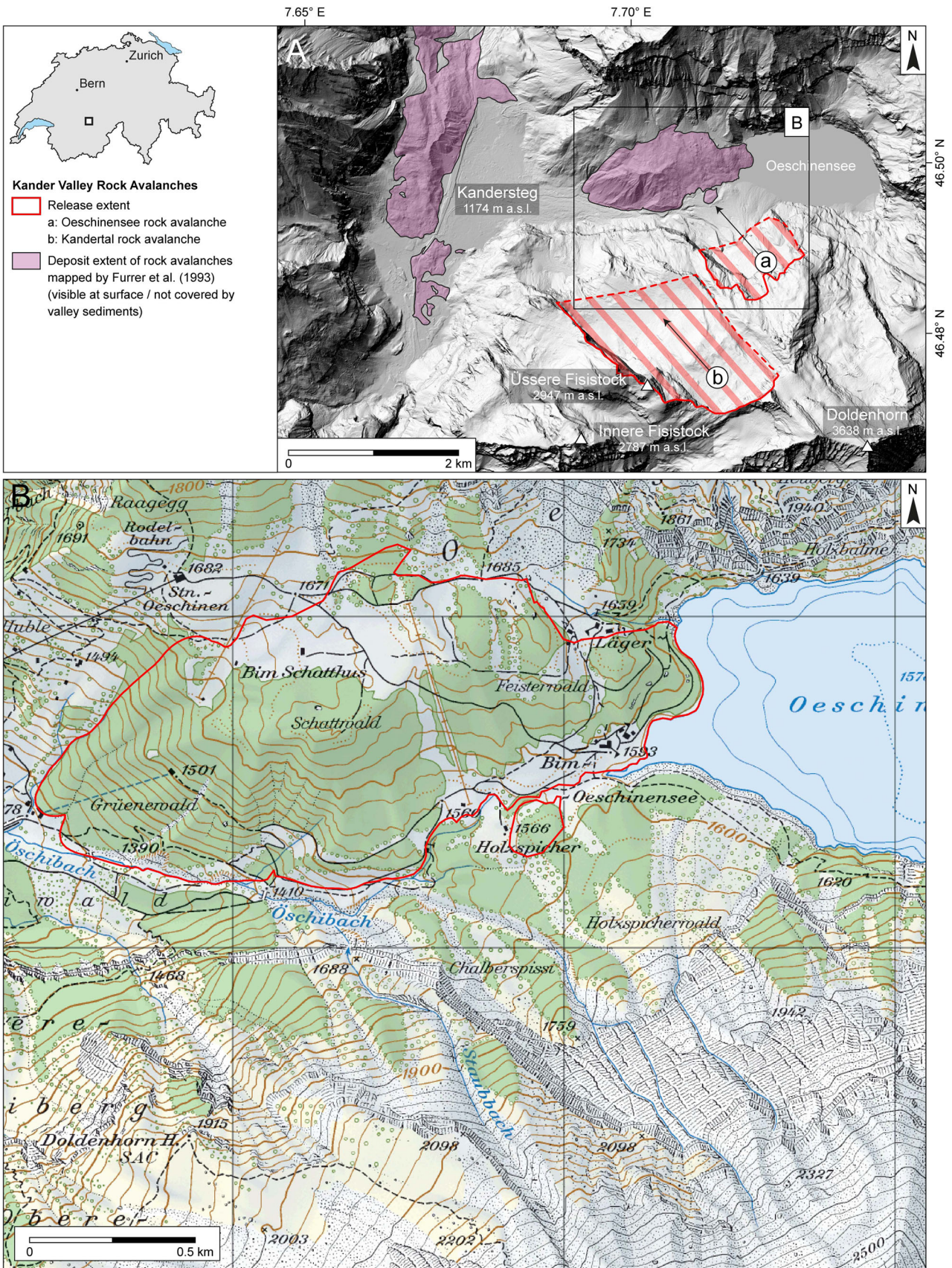
Fig. 1 **a** Overview of the study area in the Kander valley of Canton Bern, Switzerland. The Oeschinensee rock avalanche (*a*) released from the northern flank of the Doldenhorn, while the Kandertal rock avalanche (*b*) from the flank of Fisistock. **b** Extent of rock avalanche deposits mapped by Furrer et al. (1993). Map data courtesy of Swisstopo

Here we address these questions through a multi-disciplinary study including field mapping and remote landslide characterization, cosmogenic nuclide surface exposure dating of slide deposits, and numerical runout modeling to explore the extent, volume, failure processes, runout behavior, and age of the Oeschinensee rock avalanche. Our results provide a new view on the prehistoric landslide that dammed Oeschinensee, and reveal new insights on the hazards and geomorphic effects of large rock slope failures in steep Alpine landscapes.

2 Study area

Our study site is located in the Oeschinental, an approximately 5 km long tributary of the Kandertal, which begins in a large and deep glacial trough containing the Oeschinensee (Fig. 1) (Bloesch et al. 1995; Amann et al. 2014). Steep rock faces of several 3000-meter peaks surround the valley. The lake is dammed by landslide deposits on its downstream shore, which can be attributed either to the Oeschinensee rock avalanche, originating from the northern flank of the Doldenhorn, or to an older rock avalanche deposit, possibly the Kandertal rock avalanche, which originated from the eastern flank of the Fisistock (Fig. 1). Blocky debris is visible from the shoreline of Oeschinensee down to the hydropower station above Kandersteg (Figs. 1 and 2). A large alluvial fan covers and obscures the distal edge of the debris body. In some areas, the deposits are clearly visible, while in other areas, the deposits are overlain by sediments or are partly eroded (Fig. 2). Deposits are deeply incised on their western margin, cut by the Oeschibach stream (Fig. 1).

Oeschinensee is supplied by surrounding glacial streams and springs from a total catchment area of about 30 km^2 . The landslide dam blocks the ~ 50 m deep lake on its western shore and maintains a mean water level at approximately 1578 m (Fig. 2). The lake has no surface outflow; water instead percolates through permeable deposits of the rock avalanche dam emerging downstream in several springs. This subsurface drainage exits first at Holzspicher (Figs. 1 and 2), while below this spring several (temporary) springs supply water to the Oeschibach. An old riverbed, visible below a small dam created in 1849 (Turnau 1906), indicates that the lake previously had at least periodic surface outflow (Fig. 2). Significant erosion



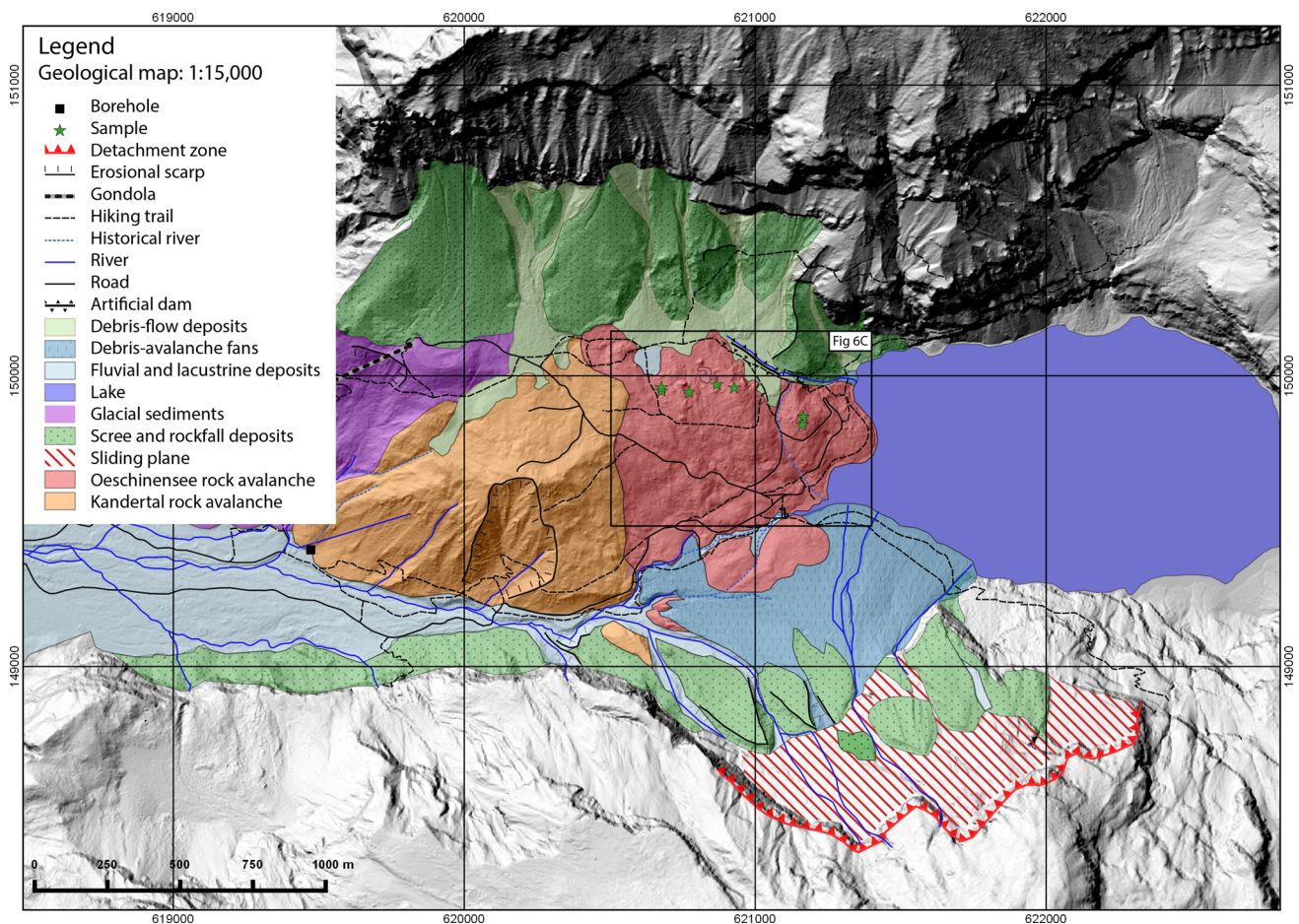


Fig. 2 Map of important Quaternary deposits in the study area, based on previous studies and independent mapping conducted in this work. Coordinates are in meters of the Swiss grid system. Topographic data courtesy of Swisstopo

of landslide deposits along the right-hand side occurred in 1846 when Oeschinensee overtopped its banks (Turnau 1906).

The most important bedrock lithologies on the southern shore of Oeschinensee belong to the Doldenhorn nappe, a folded and inverted sequence of Mesozoic sedimentary rocks (Trümpy 1980). Rocks exposed at the surface are mainly limestone with varying amounts of marl and sandstone (Fig. 3). The oldest is the Quinten Formation, a massive grey to dark grey limestone. Next is the Zementstein Formation, an inter-bedded sequence of black to medium grey marls and dark grey limestone beds (Krebs 1925). The lithology of the younger Öhrli limestone varies due to different conditions during deposition, containing dark grey oolitic limestones, limestones with sparry calcites and coral fragments, and coarse-grained and sandy limestones. Siliceous and banded limestones (Kieselkalk) form the youngest Mesozoic rocks in our study area, the Hauterivien Formation. Tertiary sedimentary rocks are only found in the highest part of the Fisistock, and consist of fossiliferous sandstones and shales (Krebs 1925).

3 Oeschinensee rock avalanche

3.1 Release area

The release area of the Oeschinensee rock avalanche is located on the northern flank of the Doldenhorn and clearly defined on two sides (Fig. 4). A large cliff forms the lateral scarp bounding the western edge of the release area. This cliff strikes parallel to prevalent northwest-southeast striking faults, which are also exposed on the sliding surface (Fig. 3). Another steep cliff forms a portion of the headscarp. This cliff is sub-vertical and ranges in height from 10 to 80 m. The northeast side of the source area is not immediately clear but can be estimated by extrapolating the cliffs above the sliding plane to the same level as the upper headscarp (Fig. 4). The highest point of the scarp is approximately 2250 m a.s.l., while to the north its height decreases to 1760 m a.s.l.

The failure surface is a sub-planar dip-slope with average inclination of 30–35° to the northwest following bedding of the Öhrli limestone (Fig. 4), which is the primary



Fig. 3 View of the release area. The basal sliding surface and head scarp are Öhrli limestone, which is overlain by the darker thinly-bedded Zementstein formation. The pinnacles are Quinten limestone (Krebs 1925)

unit incorporated in the failure. The slide also mobilized sandstones of the overlying Zementstein Formation, as well as surficial glacial deposits from the northern flank of the Doldenhorn. The shape and morphology of the evacuated region led us to hypothesize that the slide failed as a single event in a sliding mode along the basal rupture surface. The sliding plane is visible in most parts of the release area, only covered in some places by thin talus. The lower boundary of the failure surface is partly obscured by talus deposited after the rock avalanche.

3.2 Deposition area and deposit morphology

Rock avalanche debris covers an area of about $1.1 \times 10^6 \text{ m}^2$, which includes the shore of the lake, the forested areas at Holzspicherwald and Feisterwald, and the meadow of Läger (Figs. 2 and 4; see Fig. 1 for place names). Rock avalanche debris can also be observed in the lake, but it is unclear from our study how far the deposits extend under water (Fig. 5a). The total length of the deposits from south to north is $\sim 1100 \text{ m}$ and the width is $\sim 890 \text{ m}$. Vertical thickness estimated from field assessment is at maximum 100 m . The highest point is located at an elevation of 1685 m a.s.l. at Feisterwald, while the lowest point is at 1540 m a.s.l. near Holzspicher (Figs. 1, 5b).

In forested areas, the rock avalanche deposit consists of regions of large boulders (Fig. 5c), as well as areas without visible boulders but displaying typical hummocky topography (Fig. 5d). The blocks at Schattwald and Feisterwald

are of distinctly different lithologies. Boulders at Schattwald consist primarily of siliceous limestones, banded siliceous limestones and tertiary sediments; i.e., rock types that appear only on the upper flank of Fisistock. These rock types are also dominant within the Kandertal deposits (Beck 1929, 1952). Vegetation covers the sometimes strongly weathered boulders. Massive gray boulders at Feisterwald, on the other hand, are predominantly Öhrli limestone (Turnau 1906; Krebs 1925). Visible matrix consists of highly crushed and shattered rock down to silt-size with angular boulders of dark gray limestone. This distribution of rock types led us to hypothesize that at least two different rock avalanches released debris into Oeschinental. The rock avalanche debris at Schattwald most likely originated from the Kandertal event (cf. Turnau 1906), while material at Feisterwald comprises the true Oeschinensee rock avalanche deposit. Additional evidence supporting this hypothesis is the springs at Holzspicher (Fig. 2). Field observations show that several springs occur at a similar elevation, suggesting that subsurface drainage follows the contact between the underlying Kandertal and overlying Oeschinensee rock avalanche deposits. The hypothesis is further supported by our release and deposit area volume estimates for the Oeschinensee event, and by run-out modeling described later.

Other types of mass movements, such as rockfalls, debris flows and debris/snow avalanches, frequently deposit debris at the base of hillslopes along the boundaries of the rock avalanche (Fig. 5e, f). This material can be distinguished from the Oeschinensee rock avalanche

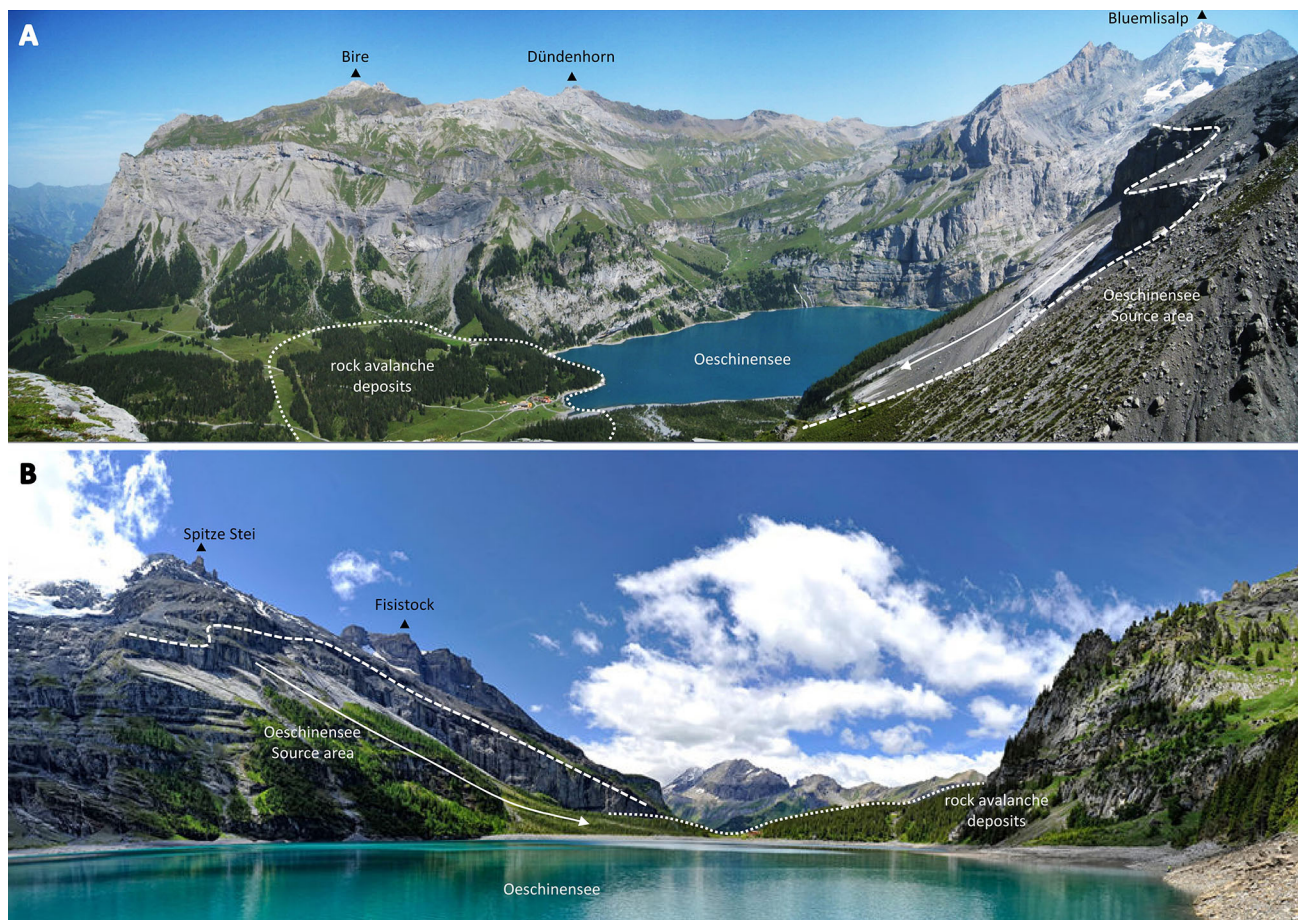


Fig. 4 Overview of the Oeschinensee rock avalanche. **a** Image of the source area (dashed line) and the deposit area (dotted line) looking north-east from the Swiss Alpine Club hut Doldenhorn. Arrow

indicates the direction of initial sliding. **b** Image of the source and deposit area seen from the eastern shore of Lake Oeschinen (view to the west)

deposit by lithology and degree of weathering. The present-day Lägerbach stream is artificially contained, but a small channel trending from Läger down to the lake reveals the former riverbed (Fig. 1). Smaller channels from the north formed ponds within the rock avalanche deposit creating flat meadows surrounded by boulders (Fig. 5f, h).

3.3 Cosmogenic ^{36}Cl surface exposure dating

Flat, intact top surfaces of ten boulders were sampled for cosmogenic dating using a battery-operated saw and hammer and chisel, based on the criteria outlined by Ivy-Ochs and Kober (2008). Positions of the analyzed boulders are shown in Figs. 2 and 6. Of these, seven were selected for analysis. Sample preparation followed procedures given by Ivy-Ochs et al. (2004, 2009) following the method of isotope dilution with addition of ^{35}Cl carrier. Total Cl and ^{36}Cl were determined at the ETH AMS facility of the Laboratory for Ion Beam Physics (LIP) with the 6 MV tandem accelerator. Measured sample ratios were normalized to the ETH internal standard K382/4N with a value of

$^{36}\text{Cl}/\text{Cl} = 17.36 \times 10^{-12}$, which is calibrated against the primary ^{36}Cl standard KNSTD5000 (Christl et al. 2013). Full process chemistry blanks ($2.2 \pm 0.8 \times 10^{-15}$) were subtracted from measured sample ratios. This amounted to a correction of less than 2% for all samples. Major and trace element concentrations, required to calculate ^{36}Cl production rates for each individual sample, were determined on an aliquot of leached sample material at XRAL (Canada) (Table 1).

Surface exposure ages were calculated with the LIP ETH in-house MATLAB code based on the parameters presented by Alfimov and Ivy-Ochs (2009; and references therein). For ^{36}Cl , we used a production rate of 54.0 ± 3.5 ^{36}Cl atoms $(\text{g Ca})^{-1} \text{ year}^{-1}$, which encompasses a muon contribution at the rock surface of 9.6% (Stone et al. 1996, 1998). For production due to neutron capture, we used a value of 760 ± 150 neutrons $\text{g}_{\text{air}}^{-1} \text{ year}^{-1}$ (Alfimov and Ivy-Ochs 2009). These values are in excellent agreement with those recently published by Marrero et al. (2016). Production rates were scaled to the latitude, longitude and altitude of the sites according Stone

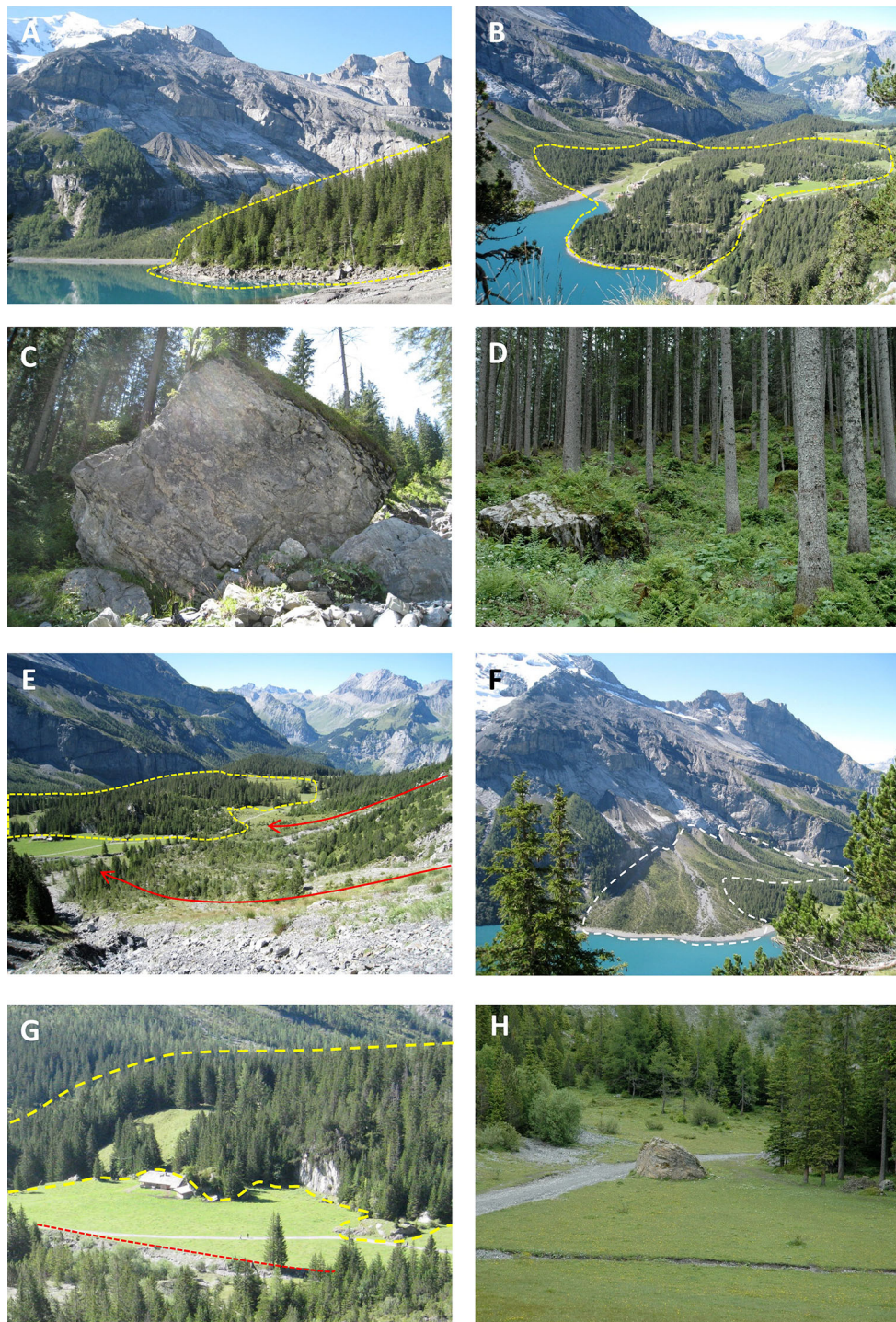


Fig. 5 Features of the rock avalanche deposit. **a** The western shore of the lake is covered with boulders, but it is unclear how far these deposits extend into the lake. **b** Rock avalanche debris covers the areas of Holzspicher, Feisterwald and Läger (see Fig. 1 for place names). **c** Large boulder at Feisterwald. **d** Hummocky topography at

(2000). No correction was made for karst weathering of the boulder surfaces. Stated errors of the exposure ages include both analytical uncertainties and those of the production rates. All determined data are shown.

Holzspicherwald. **e** Rockfall, debris-flow and avalanche deposits behind the rock avalanche at Läger. **f** Debris avalanche deposits below the failure surface. **g** Meadow surrounded by rock avalanche deposits at Läger. **h** Filled in pond within the rock avalanche deposit

Exposure ages for the Oeschinensee rock avalanche range from 2.14 ± 0.14 to 2.60 ± 0.18 kyr (Table 2, Fig. 6), with a mean age of 2.3 ± 0.2 kyr. Previously it was assumed that the Oeschinensee rock avalanche

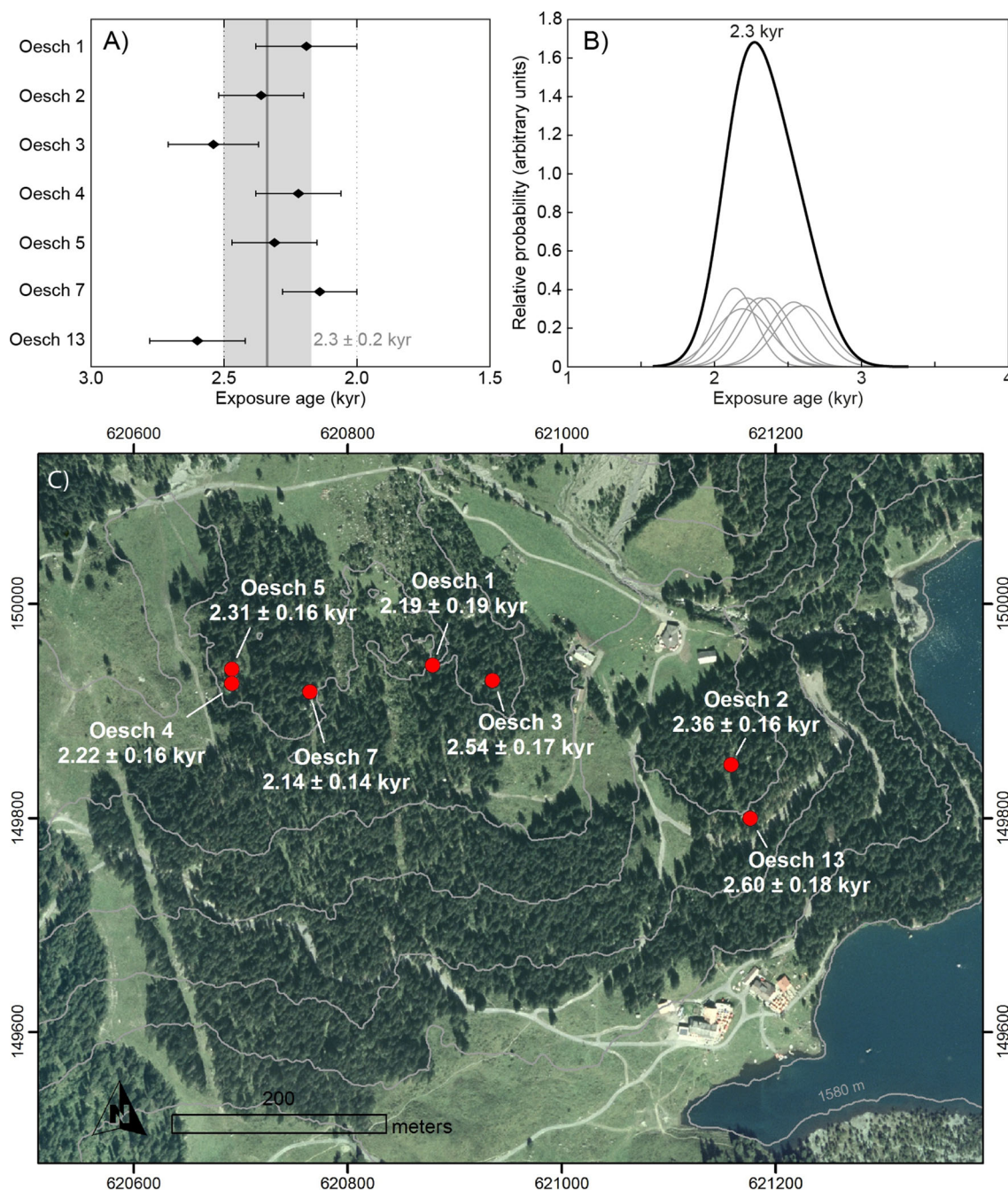


Fig. 6 **a** Cosmogenic exposure ages for the Oeschinensee rock avalanche showing a mean age of 2.3 ± 0.2 kyr (indicated in gray). **b** “Camel plots” (Balco 2011) for the Oeschinensee rock avalanche

samples showing an identical peak age of 2.3 kyr. **c** Deposit area showing the locations of samples and resulting exposure ages. The ages are consistent with a single event. Contour interval is 30 m

occurred during the early Holocene, around 9–8 kyr before present, coincident with the Kandertal event (Tinner et al. 2005) and several other large prehistoric rock avalanches in the Swiss and Austrian Alps (von Poschinger and Haas 1997; Ivy-Ochs et al. 1998, 2009, 2017; Prager et al. 2008; Grämiger et al. 2016), however our data show this is not the case. The small range of measured ages for the Oeschinensee deposit suggests exposure at the same time,

and is consistent with our hypothesis of single-event emplacement.

3.4 Reconstruction of pre-failure topography and volume analysis

Volume assessment for the Oeschinensee rock avalanche source and deposit consists of comparison between pre-

Table 1 Major element data for the analyzed samples (determined by XRF and ICP at XRAL, Ontario, Canada)

Major elements (weight %)	Oesch 1	Oesch 2	Oesch 3	Oesch 4	Oesch 5	Oesch 7	Oesch 13
SiO ₂	1.10	1.78	4.42	1.24	1.03	2.31	2.27
Al ₂ O ₃	0.22	0.30	0.93	0.27	0.14	0.54	0.86
Fe ₂ O ₃ total	0.13	0.21	0.47	0.37	0.10	0.29	0.41
MnO	< 0.01	< 0.01	0.01	0.01	< 0.01	< 0.01	< 0.01
MgO	1.12	6.39	5.49	0.58	1.00	3.56	4.10
CaO	53.50	46.20	45.90	53.70	54.70	50.20	47.70
Na ₂ O	< 0.10	< 0.10	< 0.10	< 0.10	< 0.10	< 0.10	< 0.10
K ₂ O	0.03	0.06	0.20	0.04	<0.01	0.13	0.20
TiO ₂	0.02	0.02	0.04	0.02	0.01	0.04	0.04
P ₂ O ₃	0.03	0.03	< 0.01	< 0.01	0.02	0.07	0.01
Trace elements (ppm)							
B	5	10	5	5	5	5	10
Gd	0.45	0.46	0.36	2.32	0.57	0.56	0.29
Sm	0.3	0.3	0.4	2.0	0.4	0.4	0.4
Th	< 0.1	0.1	0.3	1.5	< 0.1	0.2	0.3
U	1.83	2.01	2.48	1.05	1.08	2.01	1.71

Table 2 Surface exposure ages calculated with shielding corrections and AMS-measured concentrations of ³⁶Cl (see also Fig. 6)

Sample no.	Lat. (° N)	Long. (° E)	Elevation (m a.s.l.)	Thickness (cm)	Shielding corr.	Total Cl (ppm)	³⁶ Cl (10 ⁵ at./g)	Exposure age (years)
Oesch 1	46.5004	7.7106	1685	2.0	0.952	13.8 ± 0.2	1.698 ± 0.137	2190 ± 190
Oesch 2	46.4996	7.7143	1663	1.5	0.960	17.5 ± 0.1	1.597 ± 0.095	2360 ± 160
Oesch 3	46.5004	7.7113	1691	2.5	0.957	20.9 ± 0.1	1.773 ± 0.106	2540 ± 170
Oesch 4	46.5003	7.7082	1680	1.5	0.914	21.2 ± 0.1	1.688 ± 0.104	2220 ± 160
Oesch 5	46.5004	7.7082	1702	1.5	0.920	10.0 ± 0.1	1.769 ± 0.104	2310 ± 160
Oesch 7	46.5003	7.7091	1701	2.5	0.958	9.2 ± 0.1	1.575 ± 0.089	2140 ± 140
Oesch 13	46.4992	7.7145	1643	1.0	0.929	19.2 ± 0.2	1.758 ± 0.108	2600 ± 180

and post-failure topographies. The post-failure topography was derived from available digital elevation models (DEMs), field observations, and topographic maps. The pre-failure topography, however, had to be reconstructed by extrapolating and modifying the current terrain data in the rock avalanche source and deposit areas (Fig. 7).

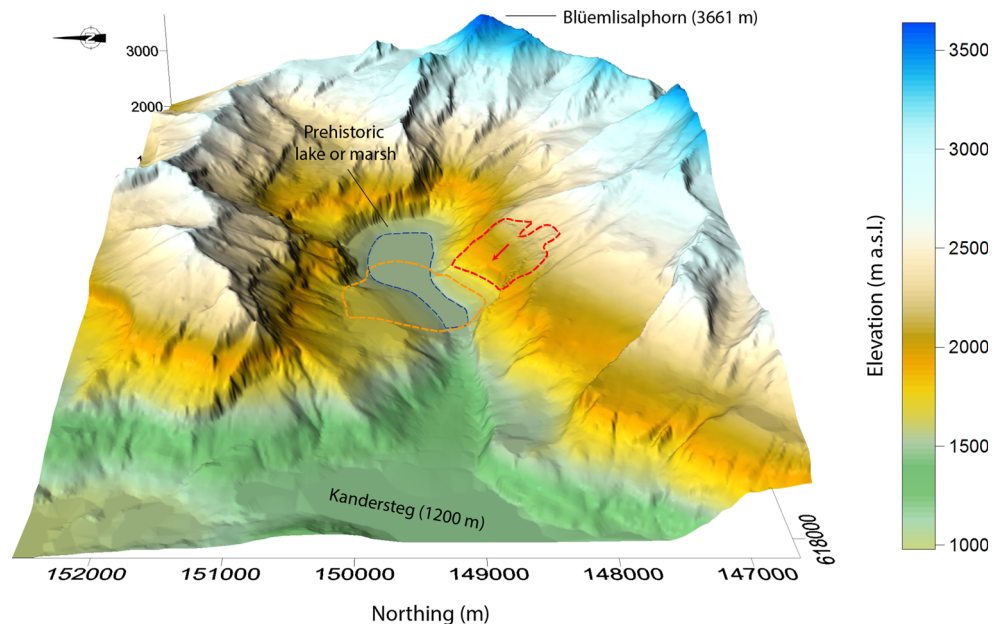
Bedrock does not outcrop at any location within the debris, and due to the unknown bedrock elevation in the Oeschinental, reconstruction of the pre-failure topography in the deposit area was challenging. From surface observations, it was almost impossible to conclusively identify the earlier valley bottom. The valley shape beneath the deposit was also not easily predicted from the surrounding terrain. Because nearby glaciers previously converged at Oeschinensee, we assumed a roughly parabolic glacial valley cross-profile. Evidence indicating the Oeschinental was over-deepened, like the nearby Gasterntal, is not available, although we believe this is likely.

To recreate the pre-failure valley topography, we clipped contour lines in the areas covered by rock avalanche

debris and redrew these with new, interpolated contour lines. Deposit modification by post-failure processes, the addition of talus on top of rock avalanche debris, as well as assumed landslide material in the lake were accounted for in a similar manner. The pre-failure topographic data were then gridded and converted into a digital surface model. We next subtracted the recreated pre-failure topography from the current DEM in order to estimate the distribution of deposit thickness (Fig. 8). The maximum estimated thickness was ~ 100 m, located just north of the source area, while deposits rapidly thin in the northwesterly direction of runout. To generate a first, rough estimate of the deposit volume (including deposits located in the lake where we have no thickness information), we multiplied the deposit area determined from field mapping (1.1 Mm²) by an assumed average thickness of 50 m; this resulted in a deposit volume of approximately 50 Mm³.

Pre-failure topography of the source area was reconstructed in a similar manner by recreating a plausible surface representing the mountain flank before the rock

Fig. 7 3D model of the pre-failure topography. Deposits of the Kandertal rock avalanche form the pre-failure runout surface of the Oeschinensee rock avalanche. The former likely dammed the Oeschinental creating a prehistoric lake or swamp (blue dashed line). Red line: rock avalanche source area with initial sliding direction indicated; orange line: rock avalanche deposit



avalanche. This was accomplished by filling in areas between the sharp western and southern scarps, and the estimated eastern and northern boundaries of the rupture surface. Overall, topographic reconstruction was better constrained in the source area as compared to the deposit. Differencing the pre- and post-slide surfaces, we determined a maximum source thickness of 225 m, an average thickness of 58 m over the 0.64 Mm^2 source area, and an estimated source volume 37 Mm^3 . This value is consistent with the crudely estimated deposit volume assuming nominal 25% fragmentation bulking as intact rock is converted to debris (Hungri and Evans 2004). Because the source area reconstruction was better constrained, we adopt the source volume of 37 Mm^3 as the best description of the event volume and thus estimate the bulked deposit volume as 46 Mm^3 .

4 Runout analysis

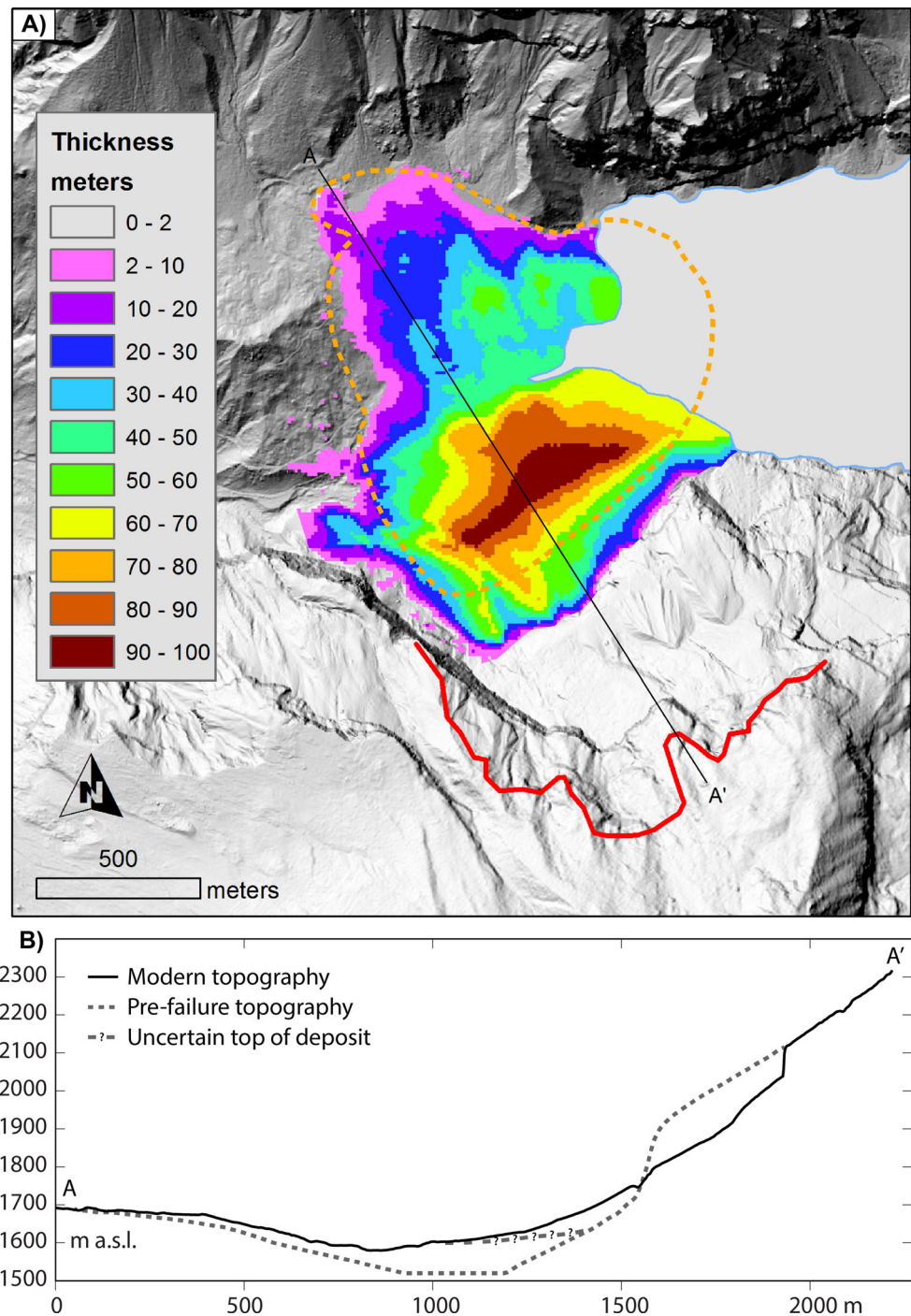
We performed 3D numerical runout simulation of the Oeschinensee rock avalanche in order to explore and confirm our hypothesized single-event failure scenario and clarify dynamic evolution of the failure and deposit emplacement. Our goal was to create a simulation that satisfactorily matched the mapped deposit extents and field-estimated thickness, using the source volume developed in the preceding analysis. We used the “equivalent-fluid” code DAN3D (McDougall and Hungri 2004; Aaron and Hungri 2016), which models rock avalanche motion over 3D terrain based on user-selection of varying rheology and basal flow resistance parameters along the runout path.

DAN3D has been successfully applied in other back-analyses of prehistoric Alpine landslides (e.g. Grämiger et al. 2016; Nagelisen et al. 2015). Due to uncertainties in our recreated pre-failure topography, we do not expect precise match to mapped deposit extents, rather we seek general agreement with the main features of the deposit.

Inputs for our simulation included grid files defining the source and path, as well as spatially assigned basal resistance parameters. We combined the recreated pre-failure topography with the present-day basal sliding plane in the source area to create the slide path. The source thickness was calculated by subtracting the recreated pre-failure source topography from the present-day sliding plane (Fig. 9). For basal flow resistance, we selected a frictional rheology and assigned a basal friction angle of 18° along the majority of the slide path, with a value of 30° in the area of the present-day lake and alluvial fan (Fig. 7). These friction angles are within the range of previously reported values for calibrated back-analyses of rock avalanches with similar volume (Hungri and Evans 1996; Sosio et al. 2011). We allowed 10 s of initial coherent motion at the start of our simulation, after which, the sliding body was instantaneously transformed into a rock avalanche (Aaron and Hungri 2016).

Results of our runout simulation are shown in Fig. 9. The failure initiates by coherent sliding along the steep dip-slope; after 10 s the body has translated roughly 130 m and is beginning to vacate the failure plane. Material travels northwest, crossing the Oeschinental and running up the opposing slope. Maximum predicted velocity of around 65 m/s occurs at ~ 20 s as the rock avalanche reaches the valley bottom. This value can be compared with the

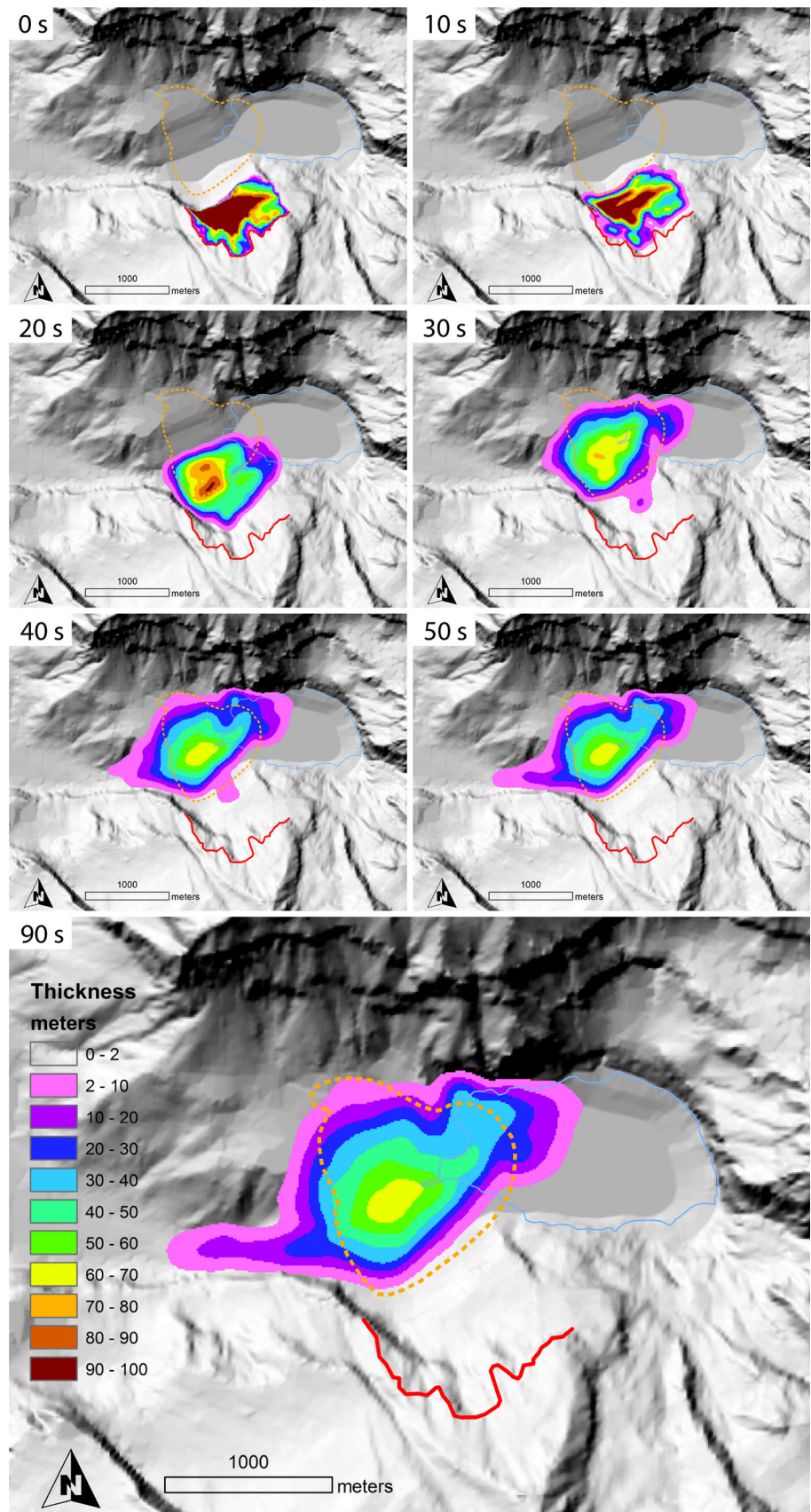
Fig. 8 a Thickness of deposits calculated by subtracting the recreated base of slide surface from present-day topography. The deposit extent is outlined in orange, red line is the failure scarp. **b** Cross-section showing the modern and pre-failure topographies, and thickness of deposits and source along the main trajectory of runout



estimated minimum velocity needed to achieve the observed runup height (h) of ~ 160 m between valley bottom and highest deposit (Jibson et al. 2006): $V_{\min} = (2gh)^{0.5}$, where g is gravity. The calculated minimum velocity estimate is 56 m/s, in good agreement with our modelled peak velocity. Between 20 and 30 s material runs up the opposing slope of the Oeschidental, and spreads laterally eastward into the area of the present-day lake. By ~ 30 s, the source area is almost completely

evacuated, and debris has begun accumulating in the proximal area of the valley. By 40 s the distal edge of the deposit has been reached, indicating an average velocity of ~ 45 m/s, and material elsewhere is beginning to come to rest. Movements after 40 s are concentrated in the steep channel sending a narrow lobe of debris down ~ 800 m toward Kandersteg. By 60 s the majority of rock avalanche movement is complete. Simulated deposits match reasonably well with our mapped deposit extent and thickness

Fig. 9 Time evolution of the Oeschinensee rock avalanche modeled using DAN3D. Selected model time steps show the thickness distribution during runout. Final simulated deposits after 90 s can be compared to field-estimated thickness (Fig. 8). The deposit extent is outlined in orange, red line is the failure scarp



distribution (Figs. 8 and 9), which show that the rock avalanche crossed the valley travelling up the opposing slope in a northwesterly direction and arrived at the southern flank of Zallershorn (Fig. 4). According to the mass distribution in the field, it appears that much of the rock avalanche turned towards the lake, while only a small amount ran down along the Oeschibach.

5 Preconditioning, preparatory and triggering factors

We distinguish several preconditioning (i.e. static and inherited, *sensu* McColl 2012), preparatory and possible triggering factors that contributed to the Oeschinensee rock avalanche. A key preconditioning factor for the Oeschinensee (as well as the Kandertal) rock avalanche is the lithological and structural setting. Bedding on the northern flank of Doldenhorn dips steeply towards the Oeschinental, creating dip-slopes along persistent bedding-parallel discontinuities. Moreover, massive limestone beds are commonly interlayered with thin beds of marl, which have weak strength properties and likely acted as preferential failure surfaces (Eberhardt et al. 2005).

A key preparatory factor for the rock avalanche was glacial erosion. Undercutting of the valley flanks during preceding glacial periods helped create a daylighting condition for otherwise slope-parallel bedding discontinuities. With retreat of Alpine glaciers following the Last Glacial Maximum, certain critically stressed slopes failed immediately, but relevant literature show that many incipient slope instabilities remained in place for thousands of years, beset by forces of frost and water pressures, earthquakes, chemical dissolution and fatigue (McColl 2012; Ballantyne et al. 2014; Grämiger et al. 2017; Ivy-Ochs et al. 2017). Together, these preparatory factors progressively weakened the failure surface of the Oeschinensee rock avalanche. The late Holocene failure age for the Oeschinensee event, however, rules out deglaciation as a direct trigger.

We identified evidence suggesting that the Oeschinensee rock avalanche was seismically triggered. The time of failure is unfortunately just before the start of historical records in Switzerland. However, studies of sedimentary deposits in Swiss lakes reveal widespread and coincident subaquatic mass movements likely associated with strong earthquakes, thus providing archives of paleo-seismicity (Leemann and Niessen 1994; Monecke et al. 2004; Schnellmann et al. 2005, 2006; Strasser et al. 2013). Significant lacustrine paleo-seismic data from lakes in central Switzerland indicate an earthquake occurred in the region around 2.3–2.2 kyr BP (Schnellmann et al. 2006; Strasser et al. 2006, 2013; Kremer, et al., 2017). This timing is identical to the age of the Oeschinensee rock avalanche

determined here (2.3 ± 0.2 kyr), and our location fits well with the likely range of possible paleoepicentres identified by Kremer et al. (2017). This suggests that the Oeschinensee rock avalanche was triggered by an earthquake in central Switzerland around 2.3–2.2 kyr BP. Seismic triggering has also been proposed for two, likely coeval rock avalanches in the nearby Rinderhorn area, although these are of early Holocene age (Grämiger et al. 2016) and likely coincident with the Kandertal event (Tinner et al. 2005). Each of these large slope failures share similar geological predisposition of steeply dipping massive limestone beds interlayered with weak marl, which may be favorable conditions for seismic triggering. Timing of the Oeschinensee rock avalanche does not coincide with several observed temporal clusters of landslides in the Alps (e.g. 10–9 kyr and 5–4 kyr; Soldati et al. 2004; Prager et al. 2008; Zerathe et al. 2014).

6 Summary and conclusions

We investigated rock avalanche deposits damming Oeschinensee in the Bernese Alps of Switzerland. Combining field and remote mapping, cosmogenic ^{36}Cl surface exposure dating and numerical runout modeling, we define the extent, volume, runout behavior, failure processes and age of the event. The lake-damming body previously mapped as a single deposit is shown by our analysis to comprise two different deposits; an older landslide in the west (likely the Kandertal event) and the Oeschinensee rock avalanche in the east. Boulder lithologies, dominance of siliceous limestone in the former and Öhrli limestone in the latter, as well as morphological character and degree of boulder weathering differentiate the two deposits. From topographic reconstruction, we calculated a volume of 37 Mm^3 for the source area and estimated a volume of 46 Mm^3 for the bulked deposit. Previous estimates were larger as they included the western Kandertal mass. The older western landslide deposits likely dammed Oeschinental such that a lake or swamp could have previously existed in the area of today's lake. Our runout modeling shows that this older deposit was necessary for the Oeschinensee rock avalanche to take the mapped travel path; i.e., we could not correctly simulate the distribution of Oeschinensee deposits without including this mass in the pre-slide topography. We modeled the failure as a single event, finding average and maximum runout velocities of 45 and 65 m/s, respectively, and adequately matching the mapped deposit extents and estimated thickness. ^{36}Cl surface exposure dating of deposited boulders reveals an age of 2.3 ± 0.2 kyr for the Oeschinensee rock avalanche. This late Holocene age is much younger than the nearby Kandertal slide (9.5 kyr) and rules out deglaciation as a trigger.

Paeoloseismic activity around 2.3–2.2 kyr BP, revealed from studies of lacustrine sediments in Swiss lakes, however, coincides with the age of the Oeschinensee rock avalanche determined here strongly suggesting a seismic trigger.

Acknowledgements We gratefully acknowledge the UNESCO World Heritage Centre, Gemeinde Kandersteg, and family Weissenfluh for financial and logistical support of field work. We thank Oldrich Hungr and Jordan Aaron for use of DAN3D, Luca Cardello for help identifying rock types, and Adrian Köpfli, Kerry Leith, and Johnny Sanders for help in the field. The AMS group at the Laboratory for Ion Beam Physics supported lab work and AMS measurements. Thanks to Michael Sturm Tomáš Pánek for helpful comments that improved this manuscript.

References

- Aaron, J., & Hungr, O. (2016). Dynamic simulation of the motion of partially-coherent landslides. *Engineering Geology*, 205, 1–11.
- Abele, G. (1974). *Bergstürze in den Alpen, ihre Verbreitung, Morphologie und Folgeerscheinungen* (p. 25). Bd: Wissenschaftliche Alpenvereinshefte.
- Alfimov, V., & Ivy-Ochs, S. (2009). How well do we understand production of ^{36}Cl in limestone and dolomite? *Quaternary Geochronology*, 4(6), 462–474.
- Amann, B., Mauchle, F., & Grosjean, M. (2014). Quantitative high-resolution warm season rainfall recorded in varved sediments of Lake Oeschinen, northern Swiss Alps: calibration and validation AD 1901–2008. *Journal of Paleolimnology*, 51(3), 375–391.
- Balco, G. (2011). Contributions and unrealized potential contributions of cosmogenic-nuclide exposure dating to glacier chronology, 1990–2010. *Quaternary Science Reviews*, 30, 3–27.
- Ballantyne, C. K., Sandeman, G. F., Stone, J. O., & Wilson, P. (2014). Rock-slope failure following Late Pleistocene deglaciation on tectonically stable mountainous terrain. *Quaternary Science Reviews*, 86, 144–157.
- Beck, P. (1929). Vorläufige Mitteilung über die Bergstürze und den Murgang im Kandertal (Berner Oberland). *Eclogae Geologicae Helveticae*, 22, 155–159.
- Beck, P. (1952). Neue Erkenntnisse über die Bergstürze im Kandertal. *Eclogae Geologicae Helveticae*, 45, 277–280.
- Bloesch, J., Hohmann, D., & Leemann, A. (1995). Die Limnologie des Oeschinensees, mit besonderer Berücksichtigung des Planktons, der Sedimentation und der Schwermetallbelastung. *Mitt. Naturf. Ges. Bern*, 52, 121–145.
- Bonnard, C. (2011). Technical and human aspects of historic rockslide-dammed lakes and landslide dam breaches. In G. S. Evans, L. R. Hermanns, A. Strom, & G. Scarascia-Mugnozza (Eds.), *Natural and artificial rockslide dams* (pp. 101–122). Berlin: Springer.
- Castleton, J., Moore, J.R., Aaron, J., Christl, M., & S. Ivy-Ochs (2016) Dynamics and legacy of 4.8 ka rock avalanche that dammed Zion Canyon, Utah, *GSA Today*, 26(6), 4–9.
- Christl, M., Vockenhuber, C., Kubik, P. W., Wacker, L., Lachner, J., Alfimov, V., et al. (2013). The ETH Zurich AMS facilities: Performance parameters and reference materials. *Nuclear Instruments and Methods in Physics Research, Section B: Beam Interactions with Materials and Atoms*, 294, 29–38.
- Costa, J. E., & Schuster, R. L. (1988). The formation and failure of natural dams. *Geological Society of America Bulletin*, 100, 1054–1068.
- Crosta, G. B., Chen, H., & Lee, C. F. (2004). Replay of the 1987 Val Pola landslide, Italian Alps. *Geomorphology*, 60, 127–146.
- Dai, F. C., Lee, C. F., Deng, J. H., & Tham, L. G. (2005). The 1786 earthquake-triggered landslide dam and subsequent dam-break flood on the Dadu River, southwestern China. *Geomorphology*, 65(3), 205–221.
- Dunning, S. A., Mitchell, W. A., Rosser, N. J., & Petley, D. N. (2007). The Hattian Bala rock avalanche and associated landslides triggered by the Kashmir earthquake of 8 October 2005. *Engineering Geology*, 93, 130–144.
- Eberhardt, E., Thuro, K., & Luginbuel, M. (2005). Slope instability mechanisms in dipping interbedded conglomerates and weathered marls—the 1999 Rufi landslide, Switzerland. *Engineering Geology*, 77, 35–56.
- Evans, S. G., Hermanns, R. L., Strom, A., & Scarascia-Mugnozza, G. (Eds.). (2011). *Natural and artificial rockslide dams* (vol. 133). Berlin: Springer
- Furrer, H., Huber, K., Adrian, H., Baud, A., Flück, W., Preiswerk, C., et al. (1993). Blatt 1247 Adelboden. *Geologischer Atlas der Schweiz*, 1, 25000. (**Karte 87**).
- Grämiger, L. M., Moore, J. R., Vockenhuber, C., Aaron, J., Hajdas, I., & Ivy-Ochs, S. (2016). Two early Holocene rock avalanches in the Bernese Alps (Rinderhorn, Switzerland). *Geomorphology*, 268, 207–221.
- Grämiger, L. M., Moore, J. R., Gischig, V. S., Ivy-Ochs, S., & Loew, S. (2017). Beyond debuitressing: Mechanics of paraglacial rock slope damage during repeat glacial cycles. *Journal of Geophysical Research—Earth Surface*, 122, 1004–1036. <https://doi.org/10.1002/2016jfg003967>.
- Heim, A. (1932). Bergsturz und Menschenleben. Beiblatt zur Vierteljahresschrift der Naturforschenden Gesellschaft in Zürich, 20, 218 pp.
- Hewitt, K., Gosse, J., & Clague, J. (2011). Rock avalanches and the pace of late Quaternary development of river valleys in the Karakoram Himalaya. *Geological Society of America Bulletin*, 123, 1836–1850.
- Hungr, O., & Evans, S.G. (1996). Rock avalanche runout prediction using a dynamic model. In K. Senneset. A.A. Balkema (Ed.), *Proceedings of the 7th International Symposium on Landslides, Trondheim, Norway, 17–21 June 1996*. Rotterdam, 233–238.
- Hungr, O., & Evans, S. G. (2004). Entrainment of debris in rock avalanches: An analysis of a long runout mechanism. *Geological Society of America Bulletin*, 116, 1240–1252.
- Hungr, O., Evans, S. G., Bovis, M. J., & Hutchinson, J. N. (2001). A review of the classification of landslides of the flow type. *Environmental and Engineering Geoscience*, 7(3), 221–238.
- Ivy-Ochs, S., Heuberger, H., Kubik, P. W., Kerschner, H., Bonani, G., Frank, M., et al. (1998). The age of the Köfels event. Relative, ^{14}C and cosmogenic isotope dating of an early Holocene landslide in the Central Alps (Tyrol, Austria). *Zeitschrift für Gletscherkunde und Glazialgeologie*, 34, 57–68.
- Ivy-Ochs, S., & Kober, F. (2008). Surface exposure dating with cosmogenic nuclides. *Quaternary Science Journal*, 57(1–2), 197–209.
- Ivy-Ochs, S., Martin, S., Campedel, P., Hippe, K., Vockenhuber, C., Andreotti, E., et al. (2017). *Geomorphology and age of the Marocco di Dro rock avalanches (Trentino, Italy)*: Quaternary Science Reviews. **in press**.
- Ivy-Ochs, S., Poschinger, A. V., Synal, H. A., & Maisch, M. (2009). Surface exposure dating of the Flims landslide, Graubünden, Switzerland. *Geomorphology*, 103(1), 104–112.
- Ivy-Ochs, S., Synal, H. A., Roth, C., & Schaller, M. (2004). Initial results from isotope dilution for Cl and Cl-36 measurements at the PSI/ETH Zurich AMS facility. *Nuclear Instruments and Methods in Physics Research*, 223, 623–627.

- Jibson, R. W., Harp, E. L., Schulz, W., Keefer, & D. K. (2006). Large rock avalanches triggered by the M 7.9 denali Fault, Alaska, earthquake of 3 November 2002. *Engineering geology*, 83(1), 144–160.
- Krebs, J. (1925). Stratigraphie der Blümlisalp-gruppe:(Fisistock–Doldenhorn–Blümlisalp–Gspalterhorn) im Berner Oberland. Gedruckt bei Stämpfli, 57 p.
- Kremer, K., Wirth, S. B., Reusch, A., Fäh, D., Bellwald, B., Anselmetti, F. S., et al. (2017). Lake-sediment based paleoseismology: Limitations and perspectives from the Swiss Alps. *Quaternary Science Reviews*, 168, 1–18.
- Kuo, C. Y., Tai, Y. C., Chen, C. C., Chang, K. J., Siau, A. Y., Dong, J. J., et al. (2011). The landslide stage of the HsiaoLin catastrophe: Simulation and validation. *Journal of Geophysical Research*, 116, F04007. <https://doi.org/10.1029/2010JF001921>.
- Leemann, A., & Niessen, F. (1994). Varve formation and the climatic record in an Alpine proglacial lake: calibrating annually-laminated sediments against hydrological and meteorological data. *The Holocene*, 4(1), 1–8.
- Marrero, S. M., Phillips, F. M., Caffee, M. W., & Gosse, J. C. (2016). CRONUS-Earth cosmogenic 36 Cl calibration. *Quaternary Geochronology*, 31, 199–219.
- McCull, S. T. (2012). Paraglacial rock-slope stability. *Geomorphology*, 153, 1–16.
- McDougall, S., & Hungr, O. (2004). A model for the analysis of rapid landslide motion across three-dimensional terrain. *Canadian Geotechnical Journal*, 41, 1084–1097.
- Monecke, K., Anselmetti, F. S., Becker, A., Sturm, M., & Giardini, D. (2004). The record of historic earthquakes in lake sediments of Central Switzerland. *Tectonophysics*, 394, 21–40.
- Murphy, J. J. (1874). Letters to the Editor: Moraines. *Nature*, 9, 202.
- Nagelisen, J., Moore, J. R., Vockenhuber, C., & Ivy-Ochs, S. (2015). Post-glacial rock avalanches in the Obersee valley, Glarner Alps, Switzerland. *Geomorphology*, 238, 94–111.
- Niklaus, V. (1967). Geomorphologische und limnogeologische Untersuchungen am Oeschinensee. Beiträge zur Geologie der Schweiz—Hydrogeologie. Schweizerische Naturforschende Gesellschaft, Nr. 14, 116 p.
- Pankow, K. L., Moore, J. R., Hale, J. M., Koper, K. D., Kubacki, T., Whidden, K. M., et al. (2014). Massive landslide at Utah copper mine generates wealth of geophysical data. *GSA Today*, 24, 4–9.
- Penck, A., & Brückner, E. (1909). *Die alpen im Eiszeitalter*. Leipzig: Tauchnitz.
- Prager, C., Zangerl, C., Patzelt, G., & Brandner, R. (2008). Age distribution of fossil landslides in the Tyrol (Austria) and its surrounding areas. *Natural Hazards and Earth System Sciences*, 8, 377–407.
- Reitner, J. M., Ivy-Ochs, S., Drescher-Schneider, R., Hajdas, I., & Linner, M. (2016). Reconsidering the current stratigraphy of the Alpine Lateglacial: Implications of the sedimentary and morphological record of the Lienz area (Tyrol/Austria). *E&G Quaternary Science Journal*, 65(2), 113–144.
- Schnellmann, M., Anselmetti, F. S., Giardini, D., & McKenzie, J. A. (2005). Mass movement-induced fold-and-thrust belt structures in unconsolidated sediments in Lake Lucerne (Switzerland). *Sedimentology*, 52, 271–289.
- Schnellmann, M., Anselmetti, F. S., Giardini, D., & McKenzie, J. A. (2006). 15,000 years of mass-movement history in Lake Lucerne: Implications for seismic and tsunami hazards. *Eclogae Geologicae Helveticae*, 99(3), 409–428.
- Soldati, M., Corsini, A., & Pasuto, A. (2004). Landslides and climate change in the Italian Dolomites since the Late Glacial. *CATENA*, 55, 141–161.
- Sosio, R., Crosta, G., & Hungr, O. (2011). Numerical modeling of debris avalanche propagation from collapse of volcanic edifices. *Landslides*, 9(3), 315–334.
- Stone, J. O. (2000). Air pressure and cosmogenic isotope production. *Journal of Geophysical Research: Solid Earth*, 105(B10), 23753–23759.
- Stone, J. O., Allan, G. L., Fifield, L. K., & Cresswell, R. G. (1996). Cosmogenic chlorine-36 from calcium spallation. *Geochimica et Cosmochimica Acta*, 60(4), 679–692.
- Stone, J. O., Evans, J. M., Fifield, L. K., Allan, G. L., & Cresswell, R. G. (1998). Cosmogenic chlorine-36 production in calcite by muons. *Geochimica et Cosmochimica Acta*, 62(3), 433–454.
- Strasser, M., Anselmetti, F. S., Fäh, D., Giardini, D., & Schnellmann, M. (2006). Magnitudes and source areas of large prehistoric northern Alpine earthquakes revealed by slope failures in lakes. *Geology*, 34(12), 1005–1008.
- Strasser, M., Monecke, K., Schnellmann, M., & Anselmetti, F. S. (2013). Lake sediments as natural seismographs: A compiled record of Late Quaternary earthquakes in Central Switzerland and its implication for Alpine deformation. *Sedimentology*, 60, 319–341.
- Suter, M. (2004). A neotectonic-geomorphologic investigation of the prehistoric rock avalanche damming Laguna Metztitlán (Hidalgo State, east-central Mexico). *Revista Mexicana de Ciencias Geológicas*, 21(3), 397–411.
- Taylor, W. A. (1893). Geographical notes. *Scottish Geographical Magazine*, 9, 477–485.
- Tinner, W., Kaltenrieder, P., Soom, M., Zwahlen, P., Schmidhalter, M., Boschetti, A., et al. (2005). Der nacheiszeitliche Bergsturz im Kandertal (Schweiz): Alter und Auswirkungen auf die damalige Umwelt. *Eclogae Geologicae Helveticae*, 98(1), 83–95.
- Trümpy, R. (1980). *Geology of Switzerland: A Guide Book* (p. 334). Basel: Part B Geological Excursions. Wepf & Co.
- Turnau, V. (1906). Der prähistorische Bergsturz von Kandersteg. Beiträge zur Geologie der Berner Alpen. Inaugural Dissertation, Universität Bern.
- von Poschinger, A., & Haas, U. (1997). Der Flimser Bergsturz, doch ein warmzeitliches Ereignis? *Bulletin für angewandte Geologie*, 2(1), 35–46.
- Wolter, A., Gischig, V., Stead, D., & Clague, J. J. (2016). Investigation of geomorphic and seismic effects on the 1959 Madison Canyon, Montana, landslide using an integrated field, engineering geomorphology mapping, and numerical modelling approach. *Rock Mechanics and Rock Engineering*, 49(6), 2479–2501.
- Zerathe, S., Lebourg, T., Braucher, R., & Bourlès, D. (2014). Mid-Holocene cluster of large-scale landslides revealed in the Southwestern Alps by 36 Cl dating. Insight on an Alpine-scale landslide activity. *Quaternary Science Reviews*, 90, 106–127.